Cation Hydration in Supercritical NaOH and HCl Aqueous Solutions

Christoph J. Sahle,[*,†] Johannes Niskanen,[‡] Christian Schmidt,[¶] Johannes Stefanski,[§] Keith Gilmore,[†] Yury Forov,[‖] Sandro Jahn,[§] Max Wilke,[⊥] and Christian Sternemann[‖]

European Synchrotron Radiation Facility, 71 Avenue des Martyrs, 38000 Grenoble, France., Helmholtz Zentrum Berlin für Materialien und Energie, Institute for Methods and Instrumentation for Synchrotron Radiation Research, Albert-Einstein-Str. 15, 12489 Berlin, Germany, Deutsches GeoForschungsZentrum GFZ, Section 4.3, Telegrafenberg, 14473 Potsdam, Germany., Institute of Geology and Mineralogy, University of Cologne, Zülpicher Strasse 49b, 50674 Köln, Germany., Fakultät Physik/DELTA, Technische Universität Dortmund, 44221 Dortmund, Germany., and Institute of Earth and Environmental Science-Earth Science, Universität Potsdam, 14476 Potsdam, Germany.

E-mail: christoph.sahle@esrf.fr,Phone:+33(04)76882711

Abstract

We present a study of the local atomic environment of the oxygen atoms in aqueous solutions of NaOH and HCl under simultaneous high temperature and high pressure conditions. Experimental non-resonant X-ray Raman scattering core-level spectra at the oxygen K-edge show systematic changes as a function of temperature and pressure. These systematic changes are distinct for the two different solutes and are described well by calculations within the Bethe-Salpeter formalism for snapshots from *ab initio* molecular dynamics simulations. The agreement between experimental and simulation results allows us to use the computations for a detailed fingerprinting analysis in an effort to elucidate the local atomic structure and hydrogen bonding topology in these relevant solutions. We observe that both electrolytes, especially NaOH, enhance hydrogen bonding and tetrahedrality in the water structure at supercritical conditions, in particular in the vicinity of the hydration shells. This effect is accompanied with the association of the HCl and NaOH molecules at elevated temperatures.

Introduction

Acidic and basic aqueous solutions contain two different forms of additional hydrogen: H^+ and OH^-, and therefore they provide fundamental information about the influence of charged particles on the hydrogen bond network of water.[1–3] Even though a wealth of studies on the specific hydration structure of the excess H^+- and OH^--ions at ambient conditions exist,[4–6]

*To whom correspondence should be addressed

†European Synchrotron Radiation Facility, 71 Avenue des Martyrs, 38000 Grenoble, France.

‡Helmholtz Zentrum Berlin für Materialien und Energie, Institute for Methods and Instrumentation for Synchrotron Radiation Research, Albert-Einstein-Str. 15, 12489 Berlin, Germany

¶Deutsches GeoForschungsZentrum GFZ, Section 4.3, Telegrafenberg, 14473 Potsdam, Germany.

§Institute of Geology and Mineralogy, University of Cologne, Zülpicher Strasse 49b, 50674 Köln, Germany.

‖Fakultät Physik/DELTA, Technische Universität Dortmund, 44221 Dortmund, Germany.

⊥Institute of Earth and Environmental Science-Earth Science, Universität Potsdam, 14476 Potsdam, Germany.

the atomic, electronic, and local structure of these species at elevated temperatures and pressures up to the supercritical regime remain largely unknown. Such information is of particular interest, as solutions of NaOH and HCl are indispensable in today's chemical industry and play a key role in geological processes.[7] Nearly all of the world's primary aluminum production is based on the Bayer process,[8] that relies on NaOH solutions of up to 320 °C and 4 MPa to form and separate $NaAl(OH)_4$ from alumina ore, bauxite. Na-rich fluids also occur in natural processes in the Earth's crust. For example, late stage hydrothermal reactions in peralkaline agpaitic igneous rocks involve NaOH as an essential component.[9] These rocks may well become the primary sources of Nb, Ta, rare-earth elements, and Zr in the future. Hot HCl-bearing aqueous fluids are of enormous importance in the upper Earth's crust, as they are responsible for the formation of many hydrothermal ore deposits such as hydrothermal tin deposits[10,11] or the giant porphyry Cu-Au deposits.[7,12] In such fluids, HCl is crucial for the enhanced metal solubility via formation of chloride complexes.

The interaction between the cation or anion and bulk water molecules was found to be very different for OH^- and H^+, but no clear details of the structural motifs could be extracted.[13,14] Optical Raman spectra of NaOH solutions in the region of the O-H stretching vibrations show very large changes with addition of NaOH.[15] However, the assignment of the extra features to stretching motions of free OH^-, $H_3O_2^-$, $H_7O_4^-$, or $H_9O_5^-$ complexes is unsettled and the impact of Na^+ and Cl^- hydration on the structure of water is not well understood at supercritical conditions.

Here, we report experimental data of the oxygen K-edge of aqueous HCl and NaOH solutions under elevated T and p conditions. The spectra show systematic changes with increasing T, p and are compared to spectra from pure neat water at similar experimental conditions. We interpret the spectral changes observed in the experiment by oxygen K-edge calculations within the Bethe-Salpeter-equation (BSE) formalism for structures from *ab initio* molecular dynamics (AIMD) simulations. In contrast to the findings at ambient conditions, and due to the strong hydration shells built around the different ions, both electrolytes enhance hydrogen bonding and increase the tetrahedral order of the water structure at the elevated temperatures and pressures studied. We also find a high degree of association of the HCl and NaOH molecules at high temperature and high pressure conditions.

Methods

X-ray Raman scattering spectroscopy

Non-resonant inelastic X-ray scattering from core-level electrons, also known as X-ray Raman scattering (XRS), allows for the investigation of shallow absorption edges using hard X-rays as a probe.[16] The use of hard X-rays makes XRS a highly bulk sensitive method without constraints on the sample environment. Thus, XRS allows for the study of the oxygen K-edge of samples under extreme conditions,[17] which is otherwise inaccessible with probes such as soft X-rays or electrons.

A typical XRS spectroscopy experiment measures the double differential scattering cross section[16]

$$\frac{\mathrm{d}^2\sigma}{\mathrm{d}\Omega \mathrm{d}\omega_2} = \left(\frac{\mathrm{d}\sigma}{\mathrm{d}\Omega}\right)_{\mathrm{Th}} S(\mathbf{q},\omega), \tag{1}$$

where $\left(\frac{\mathrm{d}\sigma}{\mathrm{d}\Omega}\right)_{\mathrm{Th}}$ is Thomson's scattering cross section, $\hbar\omega_2$ is the energy of the scattered x-rays, and $S(\mathbf{q},\omega)$ is the dynamic structure factor that holds all information about the sample obtainable by XRS. It is given by

$$S(\mathbf{q},\omega) = \sum_{\mathrm{i,f}} g_{\mathrm{i}} \left| \langle \mathrm{f} | \sum_j e^{(i\mathbf{q}\cdot\mathbf{r}_j)} | \mathrm{i} \rangle \right|^2 \delta(E_{\mathrm{i}} - E_{\mathrm{f}} + \omega), \tag{2}$$

where $\mathbf{q}$ is the momentum and $\omega = E_{\mathrm{f}} - E_{\mathrm{i}}$ the energy transferred to the sample in the inelastic scattering event, exciting the system from the initial state $|\mathrm{i}\rangle$ (weighted by its probability

g_i) into the final state $|f\rangle$. $\mathbf{r}_j$ is the position of the jth electron. In the limit of small absolute values of momentum transfer $|\mathbf{q}|$ the dynamic structure factor is directly proportional to the soft X-ray absorption spectroscopy signal.[18] Therefore XRS at small scattering angles provides near-edge X-ray absorption fine structure (NEXAFS) signal for bulk samples that is free of saturation-effects. At increased momentum transfers, XRS is furthermore sensitive to dipole-forbidden transitions and thus provides access to the entire unoccupied density of states.[19]

Experiments

Data on HCl solutions were taken at the inelastic scattering beamline ID16[20] of the European Synchrotron Radiation Facility (ESRF), Grenoble, France. The experimental setup was identical to the one used in Ref. 21. All experimental data on NaOH solutions were taken at the new inelastic X-ray scattering beamline ID20 of the ESRF using the large-solid-angle spectrometer.[22] Incident X-rays from four undulators were monochromatized by a succession of a Si(111) high heat-load- and a Si(311) channel-cut monochromator. The X-ray beam was focused down to a spot-size of approximately $50 \times 150\ \mu m^2$ at the sample position. The overall energy resolution was 0.7 eV employing 12 Si(660) analyzer crystals in the vertical scattering geometry. The experimental momentum transfers were $q = 1.6 \pm 0.2$ Å^{-1} for all HCl solutions and $q = 2.3 \pm 0.2$ Å^{-1} for all NaOH solutions. The analysis of the experimental data was achieved using the XRStools program package.[23,24] At each (p, T)-condition we measured several XRS spectra, checked them for consistency and averaged over them. All final spectra were area normalized in the spectral region between 525.0 and 555.0 eV energy loss. The experimental data of pure water was taken from Ref. 21.

High pressure and high temperature conditions were generated using a hydrothermal diamond anvil cell (HDAC) with a culet size of 1 mm. The sampled volume was located in a cylindrical recess in one of the culets (see Ref. 21). The cell was sealed by an iridium gasket. The pressures were obtained from measurement of the liquid-vapor homogenization temperature after each experiment and use of applicable correlation functions.[25,26] Starting solutions were 5 M NaOH (Merck) and a 10% HCl solution produced from doubly distilled water and a 20% HCl solution (Sigma-Aldrich). The actual HCl or NaOH concentration of the solution after loading in the sample chamber of the HDAC are usually higher due to evaporation and were determined from measurement of the freezing point depression. The sample was monitored visually during all measurements using a camera system. We collected spectra between ambient conditions and maximum p, T conditions of $p, T =$ (124 MPa, 600 °C) for 13 m NaOH, $p, T =$(346 MPa, 600 °C) for 7 m NaOH and $p, T =$ (76 MPa, 400 °C) for 4.4 m HCl.

Theory

MD simulation

The structures of liquid and supercritical NaOH and HCl solutions were simulated by AIMD using the CPMD code.[27] The simulation cells contained either 54 H_2O and 5 NaOH or 60 H_2O and 4 HCl molecules. This corresponds approximately to a 5 m NaOH and a 4 m HCl solution. All simulations were performed at constant volume and temperature, i.e. in the NVT ensemble. Densities were adjusted to those of the experiments. Temperature was controlled by a Nosé-Hoover thermostat.[28,29] For the electronic structure calculations, plane-wave basis sets, the BLYP exchange correlation functional,[30,31] and Goedecker-type pseudopotentials[32] were used. The Kohn-Sham orbitals were expanded up to an energy of 70 Ry. The equations of motion of the Born-Oppenheimer MD were integrated with a time step of 0.5 fs. The initial structures were modified from a previous simulation study of supercritical H_2O.[21] After equilibration at each state point, production runs of at least 10 ps were performed. From the recorded trajectories, partial radial distribution functions and XRS spectra were com-

puted. Stick and ball representations of typical snapshots at ambient and supercritical solutions are shown in Fig. 1.

Spectral calculations

Individual non-resonant inelastic X-ray scattering spectra were calculated for each oxygen atom of five snapshots from the AIMD production trajectories using the BSE method as implemented in the OCEAN code.[33–35] The snapshots for the spectral calculations were sampled at constant time intervals of 2 ps. Thus, in total we calculated 295, 300, and 320 individual oxygen K-edge spectra for NaOH(aq), HCl(aq) and water, respectively, for each (p, T) point. We used a momentum transfer of 3.0 Å^{-1}. For comparison with the experimental data, all spectra were convoluted with a GW self-energy obtained from a many-pole approximation to the valence level loss function[36] and a Gaussian of 0.7 eV full width at half maximum (FWHM) to account for the experimental resolution. All averaged spectra were shifted on the energy loss scale to match the experimental K-edge onsets.

Results and Discussion

The dependence of the shape of the oxygen K-edge on the structure of aqueous systems is considered mostly understood, although some details are still debated.[37] The oxygen K-edge exhibits three well recognizable features: the pre-edge, the main-edge, and the post-edge. Spectral intensity in the pre-edge region is generally connected to weakening or breaking of hydrogen-bonds and a prominent pre-edge peak can be found for example in supercritical water.[21] A prominent main-edge is commonly connected to a heavily distorted and weakly hydrogen-bonded network. Furthermore, similar changes in the main-edge have also been attributed to a density increase in which the hydrogen bonding does not necessarily change, for example, in high density ices.[38] The post-edge is prominent in the presence of tetrahedral order and a strong hydrogen-bond network. Therefore, oxygen K-edges of several ice phases exhibit larger spectral weight in the post-edge region.[38,39] This intensity behavior has to be understood as a net effect of the ensemble average rather than an effect on the spectra of individual sites, that show large structure–intensity variation in liquid water.[40]

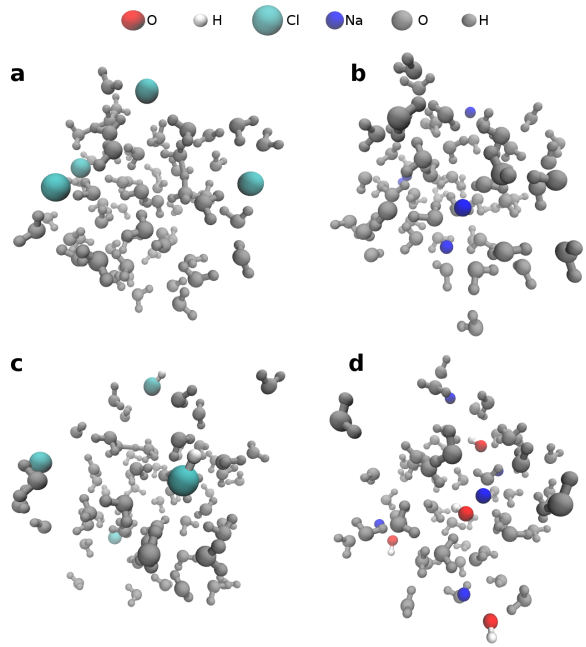

Figure 1: Snapshots from the AIMD simulation showing mainly dissociated species at ambient conditions: a) Cl^- in HCl(aq) and b) Na^+ in NaOH(aq), and the formation of contact ion pairs at high temperatures: c) HCl in HCl(aq) and d) NaOH in NaOH(aq). The ions and their contact pairs are indicated in color, the O and H atoms not involved in contact pairs are shown in grey.

Fig. 2 a)-f) presents an overview of the experimental data and the computational results (experimental data for 7 m NaOH are shown Fig. S1 in the SI). As is the case for pure water, the spectra of the HCl and NaOH solutions show a systematic temperature and pressure dependence. The pre-edge of the O K-edge (centered around 535 eV energy loss in the spectrum of the ambient samples) gains spectral weight and shifts to lower energy losses as temperature and pressure are increased. Likewise, the main-edge (around 537 eV energy loss) gains intensity and shifts to lower energy losses. The post-edge, on the other hand, prominent in the

ambient spectra at energy losses around 541 eV, loses spectral weight with increasing temperature and pressure. Following the above arguments about the general interpretation of the O K-edge in terms of the local atomic structure, all liquids show a general loss of tetrahedrality and a reduction of hydrogen-bonding as temperature and pressure increase.

The overall trends observed in the experimental data are reproduced entirely by the calculated spectra shown in the right column of Fig. 2. However, the pre-edge feature is slightly overestimated, except for pure water at ambient conditions, whereas the post-edge feature, as well as the overall width of the K-edge, is underestimated by the theory. Spectral calculations based on structures obtained from path-integral molecular dynamics rather than classical nuclei ab initio molecular dynamics have been shown to yield more accurate pre- and post-edge intensities,[41] improving the overall agreement with experiment.

In an effort to quantify the accordance of simulation and experiment, we show the integrated intensity in the pre-edge, the main-edge, and the post-edge regions as a function of temperature in Fig. 2 g)-i). Values extracted from the experimental data are shown as solid lines and those from the simulated spectra by symbols. These values were obtained by trapezoidal integration of the experimental spectra in spectral ranges pre-edge = [532.5, 535.5], main-edge = [535.5, 540.0], and post-edge = [540.0, 546.5] (all in eV), i.e. comparable to previously used integration ranges.[40] Error estimates represent standard deviations of values obtained by slightly varying these integrations ranges by up to ± 0.2 eV. The integrated pre-edge intensities of the simulation results were scaled by constant factors and show the systematic behavior also found in the experimental spectra. These scaling factors reflect the difficulty of core-level simulations for liquid molecular systems to yield perfect absolute agreement between experiment and simulation. Apart from this minor mismatch of the absolute intensities the experimental trends are reproduced impressively. A direct comparison of the spectra of pure water and the HCl and NaOH solutions at each temperature is shown in Figs. S2 in the SI and allows a direct observation of the effect the electrolytes have on the spectral shape of the oxygen K-edge.

According to the common interpretation of the oxygen K-edge of water in terms of the local atomic structure, the data recorded at higher temperatures show spectral indications of enhanced hydrogen bonding and increased tetrahedral order upon addition of HCl when compared to neat water at similar p- and T-conditions. The high-temperature spectra of NaOH(aq) show even stronger hydrogen bonding and also a noticeable tetrahedral-order signature. The number of hydrogen bonds (Fig. 3 a)), extracted from the MD simulations, supports this view: in comparison to neat water at $T > 200$ °C the water hydrogen bonding is enhanced in HCl(aq) and even more so in NaOH(aq). We likewise evaluated the deviation from tetrahedrality as defined in Ref. 40. The results for the three solutions are shown in Figs. 3 c) and d). The deviations from tetrahedral distance, in particular, are larger for pure water than for the electrolyte solutions at high temperatures. According to the simulations, the tetrahedral-order-preserving effect is greater for NaOH(aq) than for HCl(aq) (see Fig. 3 c)). These changes are also reflected by the pair distribution functions extracted from the AIMD simulations, which are shown in Figs. S3 and S4 in the SI. The number of cation-anion contact pairs per cation as extracted from the AIMD simulations based on distance criteria (the H^+-Cl^- cutoff was 1.4 Å, the OH^--Na^+ cutoff was 2.6 Å) is presented in Fig. 3 d) and shows that in the simulations both NaOH and HCl are fully dissociated at lower temperatures and pressures, but the number of contact pairs increases drastically under supercritical conditions (see also snapshots shown in Fig. 1). This observation has been reported earlier and is due to an increase in net entropy for the associated pair as compared to the ambient case and occurs because the entropy loss due to the electrostriction by water molecules is smaller for ion pairs than for free ions.[42] Our experiment is in line with this view, because we indeed see a reversal of spectral effects between 22 °C

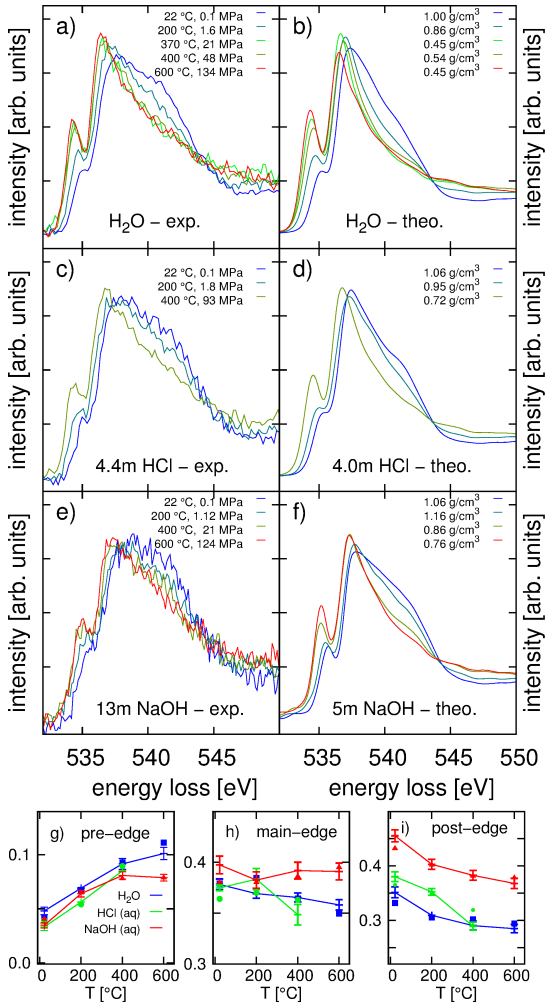

Figure 2: Comparison of experimental and computational results. a) Experimental oxygen K-edge data of pure water as a function of p and T (data taken from Ref. 21). b) Calculated oxygen K-edge spectra of pure water for similar conditions as the measured ones in part a) (structures taken from Ref. 21). c) Experimental oxygen K-edge data of 4.4 m HCl solutions at different p and T. d) Calculated aqueous HCl K-edge spectra c). e) Experimental data for 5 m NaOH solutions at various p and T conditions and f) calculated spectra for NaOH solutions. The integrated pre-edge (g), main edge (h), and post edge (i) intensities as a function of temperature. The solid lines represent the experimental values, while the symbols represent scaled values extracted from the simulated spectra.

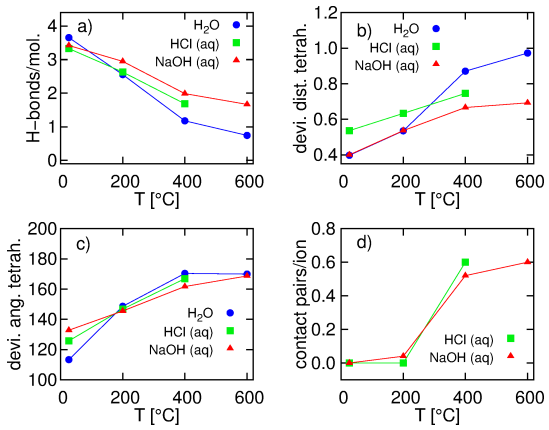

Figure 3: Structural-parameter averages extracted from the MD simulation snapshots used for the spectral evaluation: a) number of hydrogen bonds per water molecule subject to geometric criteria, b) distance-based deviation from tetrahedrality, c) angular deviation from tetrahedrality per H_2O molecule, and d) number of contact pairs per Cl^-/Na^+ ion.

and higher temperatures. Ion-pairs of Cl^- and H_3O^+ can also be identified from the MD simulations and are in line with previous findings from a combined EXAFS and AIMD study.[43]

In order to access the different spectral fingerprints present in the aqueous solutions, we extracted the spectra of the first solvation shell of the Cl^-, Na^+, and OH^- ions (including the spectrum of the central oxygen of the OH^--ion), as well as the spectra of the Eigen and Zundel motifs of protonated water from the simulation. We distinguished between Eigen and Zundel motifs subject to geometrical criteria:[44] a hydronium ion was assumed to be of Eigen type if it was solvated by three water molecules at approximately equal distance. Classification as Zundel type was based on one of the O-O distances being approximately $r = 2.4$ Å and the two remaining at approximately $r = 2.6$ Å. The spectra of these oxygen atoms are depicted in Fig. 4, their relative frequencies (fraction of water molecules in the respective hydration shells compared to the total number of water molecules in the simulation boxes) are presented in Fig. 5. For the spectra of the hydration shells (solid lines), we also plot the spectra

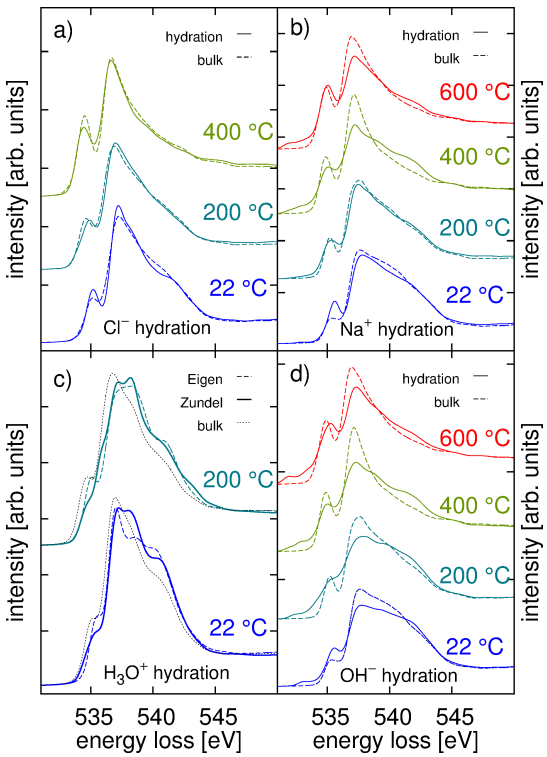

Figure 4: Calculated spectra of the hydration shell water molecules for a) the Cl^- anion, b) the Na^+ cation and spectra of the direct environment of the two types of access protons: c) the hydronium and d) the hydroxyde molecules. The OH^- hydration spectrum is constructed from the OH^- ion and its first nearest neighbors, the respective bulk spectrum was constructed from all other molecules.

of all water molecules that are not associated to any first hydration shell (dashed lines, denoted as 'bulk').

The spectra of the Cl^-- and Na^+-hydration water molecules (Fig. 4 a) and b)) show the opposite effect of what is observed in the supercritical regime for neat water: the pre-edge is reduced and the post edge-is enhanced compared to the spectrum of the bulk water molecules. The Eigen and Zundel motifs (Fig. 4 c)) are observed in the two lowest temperatures of the HCl solutions and appear more like those of neat water. The spectra of the Zundel-type motives exhibit a particularly reduced pre-edge. Both the spectra of the Zundel- and Eigen-type motives furthermore have enhanced post-edges when compared to those of neat water (thin dotted line). Throughout the entire temperature regime, the spectra of the hydroxide ions (Fig. 4 d)) and their immediate surrounding appear broader with significant weight in the post-edge region as a sign of increased tetrahedral order in their direct vicinity. This exemplifies that the observed spectral effects are due to the strong solvation-shells around the chlorine, hydronium, sodium, and hydroxide ions; the hydrogen bond structure in the bulk is vastly disturbed at supercritical conditions similar to pure supercritical water.[21]

Finally, from the fractions of water molecules in the different hydration shells shown in Fig. 5 a congruent picture emerges: in the NaOH solutions almost all water molecules are in strong hydration shells of both, the Na^+ and OH^- ions, leading to few water molecules in the bulk and an overall stabilized network. This effect is also observable in HCl(aq) but to a lesser extent. As T and p increase, more and more contact-ion pairs form that exhibit weaker hydration shells due to the charge neutralization upon the recombination.

Summary and Conclusions

We presented experimental data of the oxygen K-edge of aqueous NaOH and HCl solutions in comparison to those of neat water. Spectral calculations based on model structures from

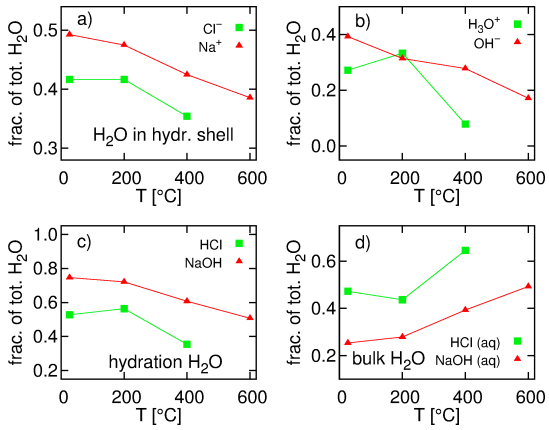

Figure 5: Estimates of the number of water molecules in the hydration shell around the Cl^- and Na^+ ions a) and the hydronium and hydroxide ions b). c) Fraction of water molecules in either hydration shell for the two electrolytes (including the hydroxide and hydronium molecules) and d) the fraction of water molecules in the bulk (*i.e. not in the first solvation shell*).

ab initio molecular dynamics simulations reproduce the experimental data and, most significantly, the systematic spectral changes observed with increasing temperature and pressure enable us to exploit the detailed atomic structural information contained in the simulation models. This combined experimental and theoretical approach reveals a crossover from a net destabilizing effect of the solvated HCl and NaOH on the water structure at ambient conditions to a net stabilizing effect of the ions at increased temperatures and pressures. This effect is due to the strong hydration shells built around the ions (Na^+, OH^-, H_3O^+, and Cl^-), which are mainly governed by Coulombic interactions, in contrast to the weaker H-bond interactions predominant amongst the bulk water molecules. At the highest probed conditions this stabilization effect is reduced slightly by an increased association of the HCl and NaOH cation/anion pairs. This is possibly due to neutralization of the charge upon recombination, which weakens the interaction with the hydration water. From a local atomic structural point of view, we observe a relatively intact water network at ambient conditions. It is incommensurate with the hydration water, which results in a net disturbing effect of the solvated electrolytes. In contrast, the hydration water largely remains unchanged at increased temperatures and pressures, but the bulk water is heavily distorted, which yields a net stabilizing effect of the solutes when compared to neat water.

Supporting Information Available: Comparison of experimental oxygen K-edge data of different NaOH concentrations; radial distribution functions extracted from the molecular dynamics runs. This material is available free of charge via the Internet at `http://pubs.acs.org/`.

References

(1) Botti, A.; Bruni, F.; Imberti, S.; Ricci, M. A.; Soper, A. K. Ions in water: the microscopic structure of concentrated NaOH solutions. *J. Chem. Phys.* **2004**, *120*, 10154–10162.

(2) Botti, A.; Bruni, F.; Imberti, S.; Ricci, M. A.; Soper, A. K. Ions in water: The microscopic structure of a concentrated HCl solution. *J. Chem. Phys.* **2004**, *121*, 7840–7848.

(3) Imberti, S.; Botti, A.; Bruni, F.; Cappa, G.; Ricci, M. A.; Soper, A. K. Ions in water: The microscopic structure of concentrated hydroxide solutions. *J. Chem. Phys.* **2005**, *122*, 194509.

(4) Marx, D.; Tuckerman, M. E.; Hutter, J.; Parrinello, M. The nature of the hydrated excess proton in water. *Nature* **1999**, *397*, 601–604.

(5) Tuckerman, M. E.; Marx, D.; Parrinello, M. The nature and transport mechanism of hydrated hydroxide ions in aqueous solution. *Nature* **2002**, *417*, 925–929.

(6) Marcus, Y. Effect of ions on the structure of water: structure making and breaking. *Chem. Rev.* **2009**, *109*, 1346–1370.

(7) Reed, M. H. Hydrothermal alteration and its relationship to ore fluid composition. *Geochemistry of hydrothermal ore deposits* **1997**, *3*, 303–365.

(8) Fifth, C. R. E. Sodium hydroxide in Ullmann's Encyclopedia of Industrial Chemistry. **2007**,

(9) Sørensen, H. The agpaitic rocks- an overview. *Mineral. Mag.* **1997**, *61*, 485–498.

(10) Schmidt, C. Formation of hydrothermal tin deposits: Raman spectroscopic evidence for an important role of aqueous Sn (IV) species. *Geochim. Cosmochim. Acta* **2017**,

(11) Duc-Tin, Q.; Audétat, A.; Keppler, H. Solubility of tin in (Cl, F)-bearing aqueous fluids at 700°C, 140 MPa: A LA-ICP-MS study on synthetic fluid inclusions. *Geochim. Cosmochim. Acta* **2007**, *71*, 3323–3335.

(12) Williams-Jones, A. E.; Heinrich, C. A. 100th Anniversary special paper: vapor transport of metals and the formation of magmatic-hydrothermal ore deposits. *Econ. Geol.* **2005**, *100*, 1287–1312.

(13) Cappa, C. D.; Smith, J. D.; Messer, B. M.; Cohen, R. C.; Saykally, R. J. The electronic structure of the hydrated proton: A comparative x-ray absorption study of aqueous HCl and NaCl solutions. *J. Phys. Chem. B* **2006**, *110*, 1166–1171.

(14) Cappa, C. D.; Smith, J. D.; Messer, B. M.; Cohen, R. C.; Saykally, R. J. Nature of the aqueous hydroxide ion probed by x-ray absorption spectroscopy. *J. Phys. Chem. A* **2007**, *111*, 4776–4785.

(15) Corridoni, T.; Sodo, A.; Bruni, F.; Ricci, M. A.; Nardone, M. Probing water dynamics with OH^-. *Chem. Phys.* **2007**, *336*, 183–187.

(16) Schülke, W. *Electron dynamics by inelastic x-ray scattering*; Oxford University Press, 2007.

(17) Sternemann, C.; Wilke, M. Spectroscopy of low and intermediate Z elements at extreme conditions: in situ studies of Earth materials at pressure and temperature via x-ray Raman scattering. *High. Press. Res.* **2016**, *36*, 275–292.

(18) Mizuno, Y.; Ohmura, Y. Theory of x-ray Raman scattering. *J. Phys. Soc. Jpn.* **1967**, *22*, 445–449.

(19) Soininen, J.; Ankudinov, A.; Rehr, J. Inelastic scattering from core electrons: A multiple scattering approach. *Phys. Rev. B* **2005**, *72*, 045136.

(20) Verbeni, R.; Pylkkänen, T.; Huotari, S.; Simonelli, L.; Vanko, G.; Martel, K.; Henriquet, C.; Monaco, G. Multiple-element spectrometer for non-resonant inelastic x-ray spectroscopy of electronic excitations. *J. Synchrotron Rad.* **2009**, *16*, 469–476.

(21) Sahle, C. J.; Sternemann, C.; Schmidt, C.; Lehtola, S.; Jahn, S.; Simonelli, L.; Huotari, S.; Hakala, M.; Pylkkänen, T.; Nyrow, A. et al. Microscopic structure of water at elevated pressures and temperatures. *Proc. Natl. Acad. Sci. U.S.A.* **2013**, *110*, 6301–6306.

(22) Huotari, S.; Sahle, C. J.; Henriquet, C.; Al-Zein, A.; Martel, K.; Simonelli, L.; Verbeni, R.; Gonzalez, H.; Lagier, M.-C.; Ponchut, C. et al. A large-solid-angle x-ray Raman scattering spectrometer at ID20 of the European Synchrotron Radiation Facility. *J. Synchrotron Rad.* **2017**, *24*, 521–530.

(23) Sahle, C. J.; Mirone, A.; Niskanen, J.; Inkinen, J.; Krisch, M.; Huotari, S. Planning, performing and analyzing x-ray Raman scattering experiments. *J. Synchrotron Rad.* **2015**, *22*, 400–409.

(24) Sahle, C. J.; Rosa, A. D.; Rossi, M.; Cerantola, V.; Spiekermann, G.; Petitgirard, S.; Jacobs, J.; Huotari, S.; Moretti Sala, M.; Mirone, A. Direct tomography imaging for inelastic x-ray

scattering experiments at high pressure. *J. Synchrotron Rad.* **2017**, *24*.

(25) Schmidt, C.; Rickers, K.; Bilderback, D. H.; Huang, R. In situ synchrotron-radiation XRF study of REE phosphate dissolution in aqueous fluids to 800 °C. *Lithos* **2007**, *95*, 87–102.

(26) Driesner, T. The system H_2O–NaCl. Part II: correlations for molar volume, enthalpy, and isobaric heat capacity from 0 to 1000 °C, 1 to 5000bar, and 0 to 1 X_{NaCl}. *Geochim. Cosmochim. Acta* **2007**, *71*, 4902–4919.

(27) Marx, D.; Hutter, J. Ab initio molecular dynamics: theory and implementation. Modern Methods and Algorithms of Quantum Chemistry. 2000; pp 301–449.

(28) Nosé, S. A molecular dynamics method for simulations in the canonical ensemble. *Mol. Phys.* **1984**, *52*, 255–268.

(29) Hoover, W. G. Canonical dynamics: equilibrium phase-space distributions. *Phys. Rev. A* **1985**, *31*, 1695.

(30) Becke, A. D. Density-functional exchange-energy approximation with correct asymptotic behavior. *Phys. Rev. A* **1988**, *38*, 3098.

(31) Lee, C.; Yang, W.; Parr, R. G. Development of the Colle-Salvetti correlation-energy formula into a functional of the electron density. *Phys. Rev. B* **1988**, *37*, 785.

(32) Goedecker, S.; Teter, M.; Hutter, J. Separable dual-space Gaussian pseudopotentials. *Phys. Rev. B* **1996**, *54*, 1703.

(33) Vinson, J.; Rehr, J. J.; Kas, J. J.; Shirley, E. L. Bethe-Salpeter equation calculations of core excitation spectra. *Phys. Rev. B* **2011**, *83*, 115106.

(34) Vinson, J.; Kas, J. J.; Vila, F. D.; Rehr, J. J.; Shirley, E. L. Theoretical optical and x-ray spectra of liquid and solid H_2O. *Phys. Rev. B* **2012**, *85*, 045101.

(35) Gilmore, K.; Vinson, J.; Shirley, E. L.; Prendergast, D.; Pemmaraju, C. D.; Kas, J. J.; Vila, F. D.; Rehr, J. J. Efficient implementation of core-excitation Bethe–Salpeter equation calculations. *Comput. Phys. Commun.* **2015**, *197*, 109–117.

(36) Kas, J. J.; Sorini, A. P.; Prange, M. P.; Cambell, L. W.; Soininen, J. A.; Rehr, J. J. Many-pole model of inelastic losses in x-ray absorption spectra. *Phys. Rev. B* **2007**, *76*, 195116.

(37) Nilsson, A.; Pettersson, L. G. M. Perspective on the structure of liquid water. *Chem. Phys.* **2011**, *389*, 1–34.

(38) Pylkkanen, T.; Giordano, V. M.; Chervin, J.-C.; Sakko, A.; Hakala, M.; Soininen, J. A.; Hamalainen, K.; Monaco, G.; Huotari, S. Role of non-hydrogen-bonded molecules in the oxygen K-edge spectrum of ice. *J. Phys. Chem. B* **2010**, *114*, 3804–3808.

(39) John, S. T.; Shaw, D. M.; Klug, D. D.; Patchkovskii, S.; Vankó, G.; Monaco, G.; Krisch, M. X-ray Raman spectroscopic study of water in the condensed phases. *Phys. Rev. Lett.* **2008**, *100*, 095502.

(40) Niskanen, J.; Sahle, C. J.; Gilmore, K.; Uhlig, F.; Smiatek, J.; Föhlisch, A. Disentangling structural information from core-level excitation spectra. *Phys. Rev. E* **2017**, *96*, 013319.

(41) Kong, L.; Wu, X.; Car, R. Roles of quantum nuclei and inhomogeneous screening in the x-ray absorption spectra of water and ice. *Phys. Rev. B* **2012**, *86*, 134203.

(42) Akiya, N.; Savage, P. E. Roles of water for chemical reactions in high-temperature water. *Chem. Rev.* **2002**, *102*, 2725–2750.

(43) Baer, M. D.; Fulton, J. L.; Balasubramanian, M.; Schenter, G. K.; Mundy, C. J. Persistent ion pairing in aqueous hydrochloric acid. *J. Phys. Chem. B* **2014**, *118*, 7211–7220.

(44) Heuft, J. M.; Meijer, E. J. A density functional theory based study of the microscopic structure and dynamics of aqueous HCl solutions. *Phys. Chem. Chem. Phys.* **2006**, *8*, 3116–3123.
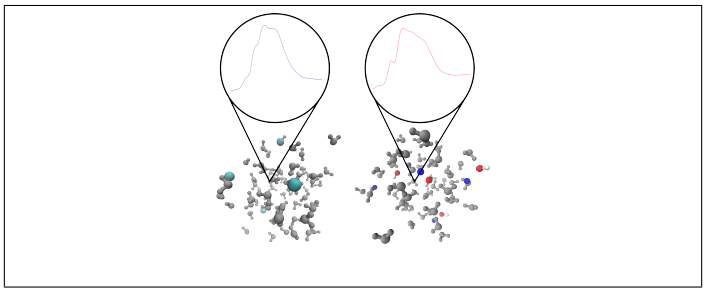
Graphical TOC Entry